Aquat. Living Resour. 24, 411–424 (2011)

DOI: 10.1051/alr/2011048
www.alr-journal.org

Aquatic
Living
Resources

Is the pearl layer a reversed shell? A re-examination of the theory of pearl formation through physical characterizations of pearl and shell developmental stages in *Pinctada margaritifera*

Jean-Pierre Cuif[1,a], Yannicke Dauphin[1], Lauren Howard[2], Julius Nouet[1], Stéphan Rouzière[3] and Murielle Salomé[4]

[1] UMR 8148 IDES, bât. 504, Sciences de la Terre, Université Paris Sud, 91405 Orsay, France
[2] Natural History Museum, Cromwell Road, London, SW7 5BD, UK
[3] UMR 8502, Physique des Solides, Bât. 510, Université Paris Sud, 91405 Orsay, France
[4] ID21, European Synchrotron Radiation Facility, BP 220, 38043 Grenoble, France

Received 4 June 2011 ; Accepted 4 October 2011

Abstract – A series of physical characterization methods (UV fluorescence microscopy, X-ray microdiffraction, backscattered electron imaging and X-ray absorption spectroscopy) were applied to Polynesian pearls collected after different cultivation periods, varying from three weeks to eighteen months. Through this rigorous time-based sampling, 120 pearls produced by 20 different donor oysters were compared. Results show that the structure of the pearl layer can be understood as a sequence of distinct secretion processes whose progressive occurrence through time may lead to variously arranged and sometimes aberrant mineralized structures. By making comparisons with the structure and growth mode of the *Pinctada margaritifera* shell, this study shows that the currently accepted theory that views the pearl-bed as a "reversed shell" cannot account for the diversity of the microstructural patterns and mineralogical properties observed in the pearl layers. From a practical and economic view point, it appears that development of these pre-nacreous materials superposed onto a perfectly round-shaped nucleus is the main cause of shape irregularities in pearls and the consequent decrease in their value.

Key words: Pearl-oyster / *Pinctada margaritifera* / Biocrystallization / Microstructural sequence / Organic matrix distribution / Layered growth mode

1 Introduction: the concept of pearls as reversed shell

It is commonly accepted that formation of the pearl layer in cultivated pearls follows a mineralization pathway comparable, in many respects, to the shell formation of pearl oysters themselves. Taylor and Strack (2008) summarized this concept of pearl layer viewed as a "reversed shell": "sections of pearls reveal that their structure is similar to the structure of the shell, the difference lies only in the reversed sequence of layers, such that the inside of the shell corresponds in its layers to the outside of the pearl". Such a view basically relies on the observations carried out by Kawakami in the early 1950s. Mostly working with *Pinctada martensi*, Kawakami noted that, in contrast to the simple scheme of pearl as a layer of nacre surrounding the spherical nucleus, the presence of non-nacreous materials is very frequent. In the method of pearl production initiated by Mise and Nishikawa in the first decade of the 20th century, the sequence of grafting operations begins by preparation of the grafts, small pieces of living tissue (about 3 × 3 square millimetres) cut from the nacre producing area of the mantle of a "donor" oyster. In a second step, each graft is deposited into the body cavity of a "receiver" oyster, with a nucleus (a sphere of biogenic calcium carbonate, usually prepared from the nacreous layer of a fresh water mollusc shell). Care must be taken to place the mineralizing surface of the graft (i.e., the external epithelium of the mantle) against the nucleus surface. Then the receiver oyster is returned to sea water and reared for two years under carefully-surveyed living conditions in order to promote optimal growth of the pearl layer.

Within the visceral cavity of the receiver oyster, the grafted fragment of mantle tissue undergoes cellular proliferation that

[a] Corresponding author: jean-pierre.cuif@u-psud.fr

leads to complete wrapping of the nucleus. This results in formation of the "pearl-sac", a complex structure whose essential component is the internal mineralizing epithelium, directly in contact with the nucleus surface. With respect to the origin of the newly formed mineralized structures, recent studies have shown that cells involved in mineralization by the pearl-sac epithelium are actually derived from the outer cell layer of the graft (Arnaud-Haond et al. 2007). Thus, formation of a nacreous layer surrounding the nucleus could be expected to be a simple continuation of the mineralizing activity of the graft before it was cut from the mantle.

In reality, however, this pattern of development rarely occurs. Kawakami (1952a, 1952b) therefore made the hypothesis that during wrapping of the nucleus by the expanding graft, cells of the mineralizing epithelium undergo important metabolic changes referred to as "regeneration", leading to formation of non-nacreous materials. Kawakami compared the organic layers visible at the base of the pearl layers with the periostracum of the shells and calcite prismatic structures frequently produced during initial mineralization of pearls, with the outer prismatic layer of the *Pinctada* shells, and finally with the nacreous layers of both pearl and shells. The results led Kawakami to conclude that, during its transformation into a "pearl sac", metabolic changes in the mineralizing epithelium resulted in formation of a new mineralization sequence, comparable to the structure of the shell itself. As this hypothetical new sequence started from the nucleus surface, it led to the concept of the pearl layer as a "reversed shell".

As pearls are of high economic importance, formation of nacre has been intensively investigated for decades, from both structural and biochemical points of view (e.g., Tsukamoto et al. 2004; Nudelman et al. 2008; Suzuki et al. 2009; Inoue et al. 2011). Recent studies on genomic expression associated with nacre production have underlined the high complexity of this biomineralization mechanism (see Joubert et al. 2010 for review). With respect to the validity of Kawakami's hypothesis though, formation of the calcite prisms, which make up the outer layer of the *Pinctada* shell, must also be taken into account. Although calcite prisms have been relatively less studied than nacreous tablets, recent studies have emphasized the leading role of organic components (proteins, polysaccharides and lipids) in their formation (Dauphin 2003; Baronnet et al. 2008; Okumura et al. 2010; Farre et al. 2011).

Based on Polynesian pearls, provided by a number of different producers, a first examination of the basal pearl layers was made in order to assess their actual level of microstructural diversity (Cuif et al. 2008). An on-going long term experimental program in French Polynesia offers the opportunity to make a developmental investigation through a series of samples taken over time. This comparative study of sizes, shapes, spatial arrangements and crystallographic status of the surprisingly diverse pearl components, each of which varies through time, provides a large database for re-examination of the current concept of pearl formation.

2 Materials and methods

2.1 Materials

Pearls were produced at the Polynesian "*Centre des Métiers de la Nacre et de la Perliculture*" at Rangiroa (Tuamotu). Receiver oysters (n = 1952) were grafted on November 20–21, 2008. All the grafting operations were made by two professional grafters only, in order to reduce influence of diversity in grafting technique. Grafts were prepared from 40 different donor oysters belonging to the *Pinctada margaritifera* (the "black lip" pearl oyster) sub-species *cumingi*, which is used in all production sites in Polynesia. All receiver oysters were grown in similar conditions in the Rangiroa lagoon. Pearls were collected after growth periods ranging from 21 days to 18 months, resulting in parallel growth series of pearls, each of known growth duration. Of these growth series, 20 were dedicated to microstructural investigations. Owing to nucleus rejections, which occurred at the usual rate, microstructure of the pearl bed was studied on 120 pearls. At the Orsay laboratory, pearls were cut using a 0.3 mm thick 150 mm diameter diamond saw at very low grinding speed (about 2 rotations/min) with a water-cooled grinding surface. Polishing of the resulting surfaces was carried out using the decreasing-grade series of the Buehler products, up to colloid silica. Only water was used as a suspension medium during grinding and polishing processes. The polished surfaces were studied using the methods described below, performed as far as possible in such an order that data could be obtained from the same area of the pearl bed.

2.2 Methods

Optical microscopy included observation by transmitted light (natural and crossed-nicol polarization), reflected natural light, UV epifluorescence by mercury lamp light filtered by UV (365 nm) and blue (435 nm) filters using both Zeiss Standard Universal epi-illumination and a Leica TCS-NT SP inverted microscope.

Microbeam X-ray diffraction measurements were carried out at the *Laboratoire de Physique des Solides* (Paris-Sud University) using a laboratory-built micro-diffraction instrument (Rouzière et al. 2010). In this equipment, X-rays are produced by a rotating-anode generator working at 40 kV and monochromatized at Cu-Kα energy (8.04 keV). The microbeam is defined by a pinhole of 20 µm diameter placed 2 mm in front of the sample, resulting in a 25 µm circular surface of the sample being submitted to X-ray for the whole measurement. Micro-diffraction mapping over the sample is performed with two motorized translation stages along the horizontal and vertical axes, with a 50 µm incremental step. The diffracted signals are collected by a CCD camera positioned behind sample and beamstop.

Micro-XANES mapping (X-ray Absorption Near Edge Structure spectroscopy), Biochemical mapping was carried out

at the ID21 beamline of the European Synchrotron Radiation Facility. The ID21 Scanning X-ray Microscope uses Fresnel zone plates as focusing optics to generate a submicron X-ray probe. An energy-dispersive high-purity Ge detector (Princeton, Gamma-Tech) mounted in the horizontal plane, perpendicular to the beam, collects the fluorescence emission photons. This geometry minimizes the contribution of elastic scattering. An energy range between 2 and 7 keV is available, which gives access to the sulphur K-edge at 2 472 eV (sulphur in amino acids) and 2 482.5 eV (sulphated sulphur in polysaccharides). For methodological examples of identification in biominerals, see Cuif et al. 2003, Dauphin et al. 2003a, 2003b. The XANES energy scan around the sulphur K-edge is achieved using a fixed-exit double-crystal Si (111) monochromator located upstream from the microscope, which provides the required energy resolution. The present experiment required the X-ray microscope to be operated under vacuum to avoid the strong absorption of the sulphur emission lines by air.

Scanning electron microscope (SEM) observations were carried out using a Philips XL30 equipped with a secondary electron and backscattered electron (BSE) detectors. In this technique, imaging contrast is due to the difference in BSE ratio, which depends on the atomic number of the atoms composing the substrate material. Thus, using a 30 kV acceleration voltage and a maximum detector contrast, BSE method provides very readable pictures emphasizing the distribution of organic envelopes and calcium carbonate phases.

X-ray computed tomography (CT) of pearl samples was performed at the Natural History Museum, London. In this method, data on pearl layers are obtained through a three-step process:

(1) The collection of a series of 2D X-ray projection images, by rotating the sample in the X-ray beam (cone-beam) by 0.1 degree increments over 360 degrees. The Metris X-Tek (Nikon Metrology) HMX ST 225 micro-CT system was used, with a 4M pixel Perkin-Elmer detector (voxel size 7.8 µm). X-rays were produced by focusing a 190 kV, 225 µA electron beam onto a molybdenum target.
(2) The 2D X-ray projection images are reconstructed into a stack of serial 2D slices using the cone-beam back projection algorithms in Nikon Metrology CT-Pro software.
(3) Rendering of the three dimensional structure of the sample is done by assembling the separate 2D slices into a single 3D volume using VGstudiomax 2.1 software. This software allows adjustment of the original rotation axis of the sample and acquisition of X-ray sections at any chosen orientation.

3 Results

3.1 The early mineralization patterns observed on the D+21 pearl layers

Most of the nuclei collected 21 days after grafting were completely covered by the very first secretions of the mineralizing epithelium, indicating that wrapping of the nuclei was already completed after three weeks (Figs. 1a–f). Many of these 20 to 30 µm thick organic coatings (Fig. 1g) exhibited colour heterogeneity: brown areas of varying colour intensity had developed over different proportions of the surface. Fragments of these early deposits could be detached from the nucleus surface (Fig. 1h). Interestingly, polarized light revealed the presence of mineral materials within these mostly organic layers. Some samples (Figs. 1i–k) clearly show two distinctly different areas with respect to polarization. Rotation of the sample (Fig. 1i) shows that some mineral components are rather consistently oriented from crystallographic view point (Figs. 1j, k). Simultaneously, neighbouring areas of the same coating fragment do not show consistent extinction.

There was considerable diversity in these early mineral depositions. Sometimes, rather large areas are covered by well crystallized spots (Figs. 1l–q), with closely comparable morphological pattern and micro-granular structure. Contrastingly, other sectors showed a patchwork of very distinctly polarizing and irregularly distributed areas (Fig. 1r). As optical identification of Ca-carbonate polymorphs using polarizing microscope is not possible, microbeam X-ray diffraction was used to precisely identify the location of the mineral phases produced at these early developmental stages.

3.2 Localized characterization of the mineral phases by microbeam X-ray diffraction

Linear series of X-ray diffraction diagrams were produced to give precise information about the diversity of the crystallization status in the mineralized areas in the 21-day-old pearl layers. Detached fragments of the nucleus cortex were fixed at the tip of a needle sample-holder and moved in front of the beam source (Figs. 2a, b). The resulting series of X-ray diffraction diagrams are obtained from interaction between the 20–25 µm diameter X-ray beam and the mineralized areas of the nucleus cortex (Figs. 2c to 2i). In this example, which is fully representative of several tens of measurements, the six recorded diagrams form a series, starting with aragonite, in which diffraction of randomly-oriented microcrystals results in circular rings of small spots (Fig. 2d), then, the three successive steps in crystals of calcite (Figs. 2e–g). In these calcite areas, diffracted beam spots are well grouped showing that calcite crystalline units are more consistently oriented (see also Fig. 3).

The simultaneous occurrence of calcite and aragonite, produced by the mineralizing epithelium in its early secretion stages, is very surprising. The validity of this observation can be assessed by examining the microbeam X-ray diffraction diagrams in more detail. Figure 3a shows one of these diagrams, in which calcite and aragonite materials are simultaneously present in the 25 µm diameter analysis spot of the microbeam diffraction instrument. The centre of the diagram shows the area where the incident beam hits the sample. For a given X-ray wavelength, crystallized minerals present in the X-ray incident area produce a diffracted beam each time their atomic lattice plans are in the Bragg position with respect to the direction of

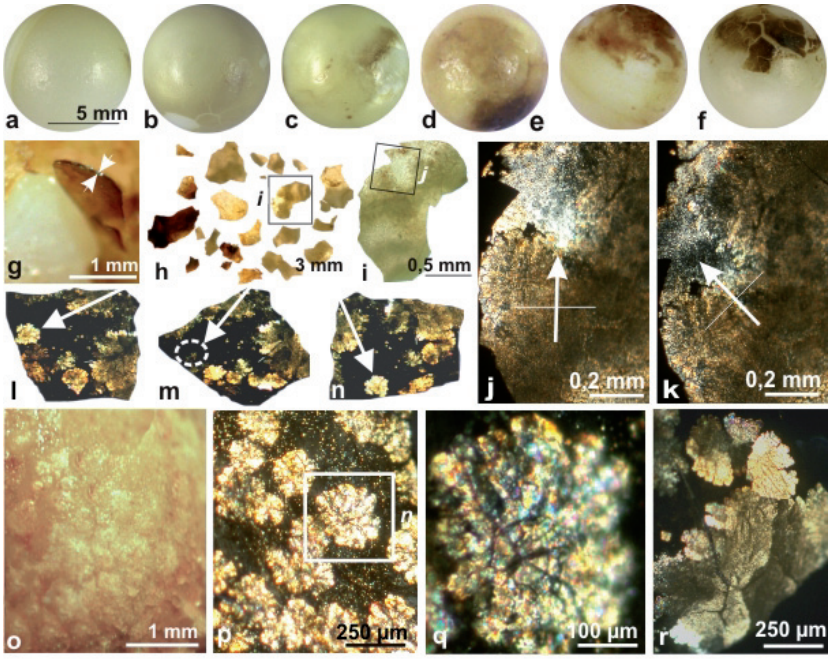

Fig. 1. Very first mineral depositions 21 days after nucleus grafting. 1a–f: surface of six nuclei illustrating colour heterogeneity of the coating. 1g, h: coating can be separated from nucleus surface (specifically the brown parts). Thickness between tips of the arrows is about 30 µm (1g). Detached fragments from a single nucleus, illustrating colour diversity (1h). 1i–k: mineralized areas of the early coating. This fragment (1i) comprises areas with distinct polarization behaviour. The mineralized sector of the upper-left part of the field view is sensitive to rotation of the microscope stage (Figs. 1j, k: arrows): mineral units of this sector change from clear to black, whereas lower part of the sector remains apparently insensitive to rotation (see below: X-ray microbeam characterization). 1l, m: example of mineralizing areas producing patchy microcrystalline units. 1l–n: rotation of a mineralized fragment observed under polarized light. Extinction of the unit (1m: arrow) during rotation from 1l to 1n reveals its cristallographic unity. 1o: surface morphology. The flat round-shaped spots are clearly visible. 1p, q: part of the same area observed in natural transmitted light (1p) between cross nicols (1q). Despite extinction under polarized light, each round-shaped unit seems to be microcrystalline. 1r: example of mineral deposition with a "patchwork" pattern: each of these distinct mineralized areas can be characterized by microbeam X-ray diffraction.

the incident X-ray beam and the used X-ray wave-length. The resulting diffracted beams diverge from the initial beam direction and hit the camera screen. Figures produced by positions of the resulting black dots provide information about two basic properties of the minerals. Distances of the spots to the diagram centre (e.g., Fig. 3a: R1, R2, R3) allow calculation of the angle between incident and diffracted beams, taking account of the distance between the sample and the screen. Compared to reference diagrams, each angle can be related to a specific lattice plan for a given mineral (see Fig. 3b).

Calcite and aragonite exhibit very different status with respect to orientation of the crystalline units (Fig. 3a). Diffracted beams located at the R3 distance (calcite) are grouped into discrete spots, whereas diffracted beams at the R1 and R2 distances from the centre are oriented in different ways, forming two quite distinct circles. These two distinct diffraction patterns indicate that in the sample area submitted to incident X-ray beam (about 25 µm in diameter) calcite crystals were rather well oriented, leading to formation of small angle crescents, whereas aragonite was made of randomly oriented microcrystalline units.

This differential result for calcite and aragonite confirms previous observations carried out using polarized light. For instance, contrast was noted between areas that were visually sensitive or insensitive to rotation of the sample between crossed nicols (Figs. 1j, k). X-ray diffraction showed that rotation sensitive zones are made of larger crystals, now known to be calcite, whereas apparently insensitive areas are built by randomly oriented microcrystals of aragonite. Here, owing to random orientation of micro-crystals, a rather constant proportion of these microcrystals were extinct or clear during rotation, causing apparent insensitivity to rotation.

However, even in calcite areas, diffraction spots may not be so well grouped (e.g., Fig. 2g), forming more or less extended crescents. In this short series, the 2h diagram shows both calcite and aragonite diffraction spots. Keeping in mind a diameter of 20–25 µm for the incident X-ray beam, we can see that it was certainly located on the limit between two distinct crystallization areas.

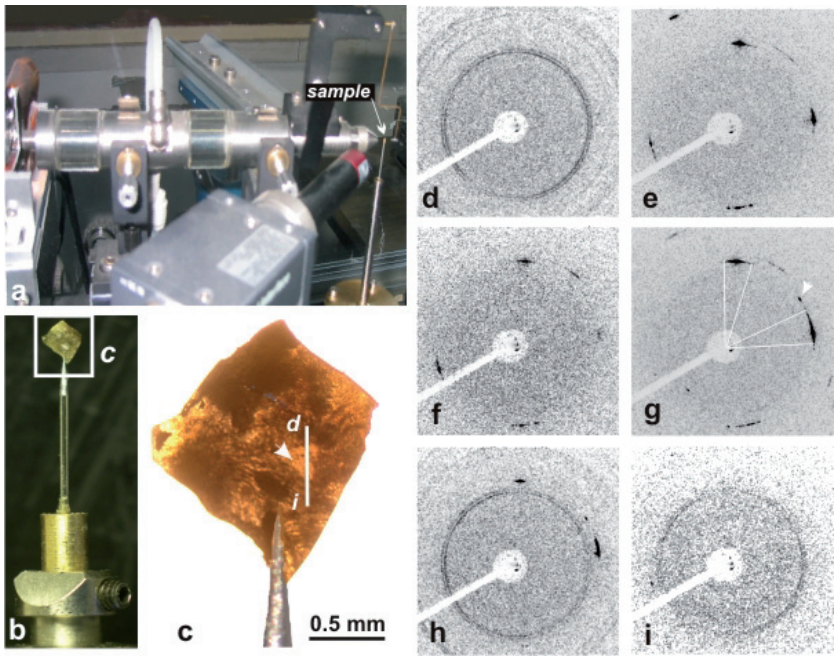

Fig. 2. Localized characterization of the mineralized areas using X-ray microbeam. 2a: X-ray beam exit tube and position of the sample in front of the exit pinhole diaphragm. 2b: Sample holder. 2c: example of a sample. 2d–i: X-ray diffraction diagrams. A clear contrast exists between the ring diagrams (2d, h, i), in which diffracted X-rays form a continuous cone intersecting the CCD screen, and the spot diagrams (2e, f, g), in which the diffracted X-rays are concentrated into restricted area. Remarkably, ring diagrams always correspond to aragonite whereas the more consistently oriented crystals (spot grouped into small crescent diagrams) correspond to calcite.

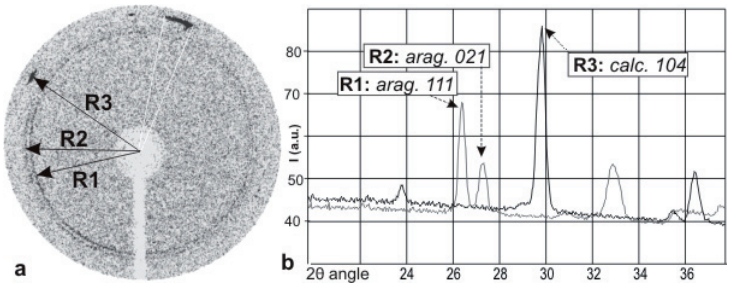

Fig. 3. In situ characterization of mineralogy and orientation of the crystalline units by microbeam diffraction diagrams. Circular diffraction patterns (R1, R2) or spotty patterns (R3) result from the presence of randomly or consistently oriented crystals, respectively (3a). Recognition of specific lattice plans is possible by calculation of each diffraction angle compared with reference diffraction diagrams for reference minerals (3b).

3.3 Two-month old pearls: occurrence of microstructural units due to formation of organic envelopes

Surfaces of pearls collected after two months of growth frequently show a surprising colour pattern (Fig. 4a). Two distinct areas are visible, forming intricate sectors that are distributed in a quite distinct manner from one pearl to another. Sections perpendicular to the pearl surface show that the thickness of pearl layers is usually between 200–250 µm. Transversal sections of the pearl layer allowed us to establish the relationship between the limits of the two distinct surface areas and the structure of the underlying mineral layers (Figs. 4a–c). The contact line between the two surface areas (Fig. 4b: *cl*) continues into the pearl layer itself. This is more important than a simple difference in colour, as a contact surface exists here (Fig. 4c: *cs*) that separates two biomineralization domains with clear cut differences in mineralogy and microstructure.

Applying microbeam X-ray diffraction on such dual sectors, a linear series of spots (Figs. 4d–l) results in an additional occurrence of the contrast between status of the calcite and

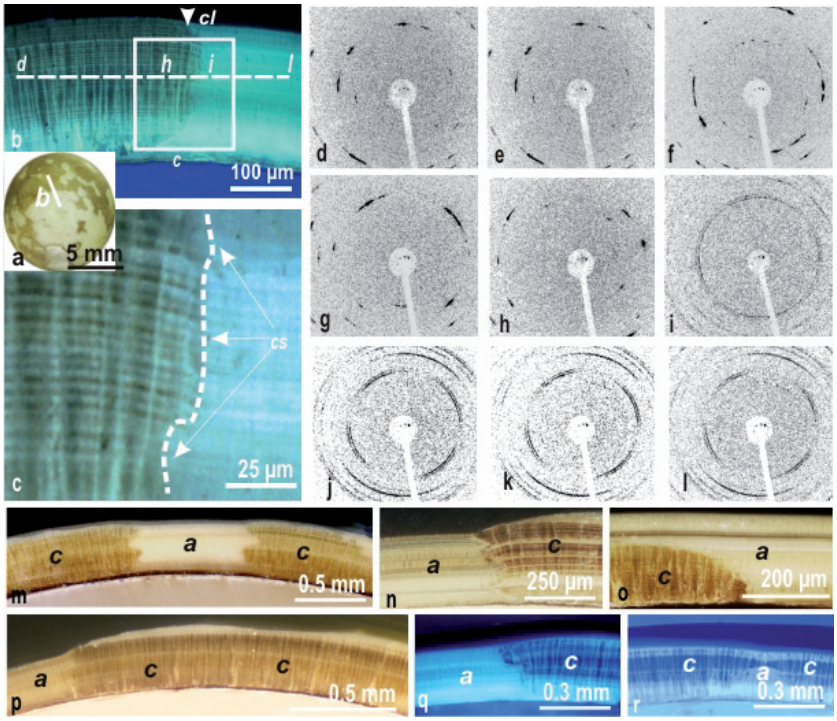

Fig. 4. Mixed basal pearl layers built of both calcite and aragonite. 4a: surface of a two-month old pearl. Irregular distribution of the fluorescence colours suggests compositional differences in areas separated by the contact line (*cl*). 4b, c: sections perpendicular to the pearl surface. Differences between adjacent areas are also structural: the radial units are very distinct between the two domains. 4d–l: series of microbeam X-ray diagrams (see location in Fig. 4b). 4d to 4h: diversely oriented calcite crystals. Figures 4j to 4l correspond to weakly controlled aragonite microcrystals: diffraction diagrams are not perfectly circular but have very large crescents (also see discussion). 4m–r: examples of mixed basal layers. Aragonite- or calcite- producing areas show irregular distributions.

aragonite areas. Calcite shows a diffraction diagram made of short crescents formed by crystals with only slight differences in orientation, whereas aragonite areas show very large crescents with close to perfect powder diffraction circles. This result is rather comparable to what was shown in the very early mineral depositions but, at two months, optical observations (Figs. 4b, c and 4m–r), UV fluorescence (Fig. 5a) and BSE imaging (Fig. 5b) show that radial envelopes are now produced, resulting in well characterized prismatic structures.

Closer observation of the contact surface (Fig. 5a: *cs*, triangular arrows) reveals continuity of the growth lines between calcite and aragonite areas (Fig. 5a: *gl*, elongated arrows). On the other hand, backscattered electron imaging shows up the radial envelopes. In both calcite (left area of the field view) and aragonite (right) sectors, organic envelopes produce radial microstructures (i.e., perpendicular to the nucleus surface; Fig. 5b) just above the initial nucleus cortex.

In the same sector, mapping of protein and polysaccharide sulphur (Figs. 5c, d) by synchrotron-based X-ray absorption (XANES peak) provides clear-cut evidence of correlation between mineralogy and distribution of the two forms of sulphur. After the initial layer (Figs. 5b, d, *il*), mostly made of protein, radial organic envelopes appear synchronously on both sides of the contact line. It should be noted that these envelopes are made of protein in both sides but, as shown in Figure 5b (and much better by a closer observation in Fig. 9), envelopes of calcite and aragonite prisms are morphologically distinct. An enlarged view of the contact line between the calcite and aragonite sectors (Fig. 5e) confirms that there is perfect continuity between growth layers in these two areas. Through conjunction of the four methods applied to the same sector (5a: laser confocal fluorescence; 5b: BSE imaging; 5c, d: XANES mapping; 5e: SEM observation), Figure 5 provides a consistent illustration of the cyclical mineralizing activity of the pearl-sac epithelium, which produces calcite and aragonite areas side-by-side within each growth layer.

3.4 The shift to nacreous mineralization: from immediate production of nacre a delay of several months

Depending on duration of the production of mixed prismatic layer, occurrence of the nacreous layer in pearl development was delayed for a variable length of time, with examples at both extremes. Nacreous tablets were sometimes produced immediately above the initial organic layer first deposited onto

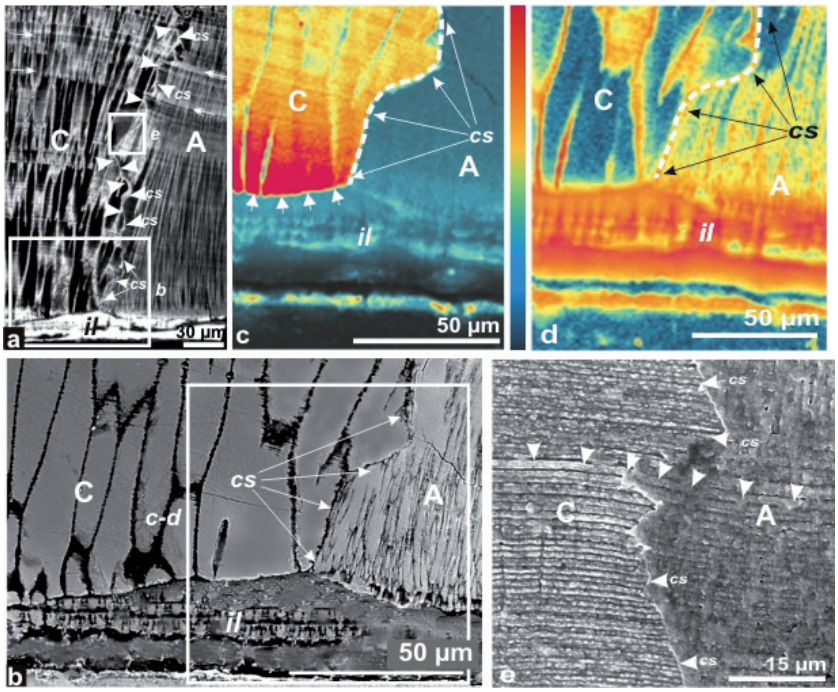

Fig 5. Calcite and aragonite prisms. Correlation with protein and acidic polysaccharide sulphur. 5a, b: section perpendicular to nucleus surface. In this field of view, the contact surface (cs, triangular arrows) separates two distinctly prismatic sectors. Envelopes perpendicular to nucleus surface are cut in their length. Note that the radial envelopes in the calcite (left) and aragonite (right) areas differ with respect to morphology, noticeably the width (i.e., diameter) of the microstructural units. This difference is much more visible on the BSE picture (5b) of the same sector. 5c, d: XANES distribution maps of protein and polysaccharide sulphur in the two prismatic sectors, as shown by X-ray absorption mapping. The large calcite prisms comprise an acidic polysaccharide component that does not exist in the aragonite sector. Note the thick basal layer (mostly protein), as well as organic envelopes, protein in both calcite and aragonite areas. 5e: growth layers exhibit a remarkable continuity when passing from calcite to aragonite sectors through the contact surface (cs).

the nucleus (Fig. 6a). At the other extreme, formation of calcite prisms could continue throughout the cultivation period, resulting in several millimetre-long units (see also Fig. 8).

While it would be superfluous and impractical to describe the huge diversity of radial organic structures built by coalescence of the organic compounds produced by the pearl-sac epithelium during this early secretion phase, the mode of apparition of the horizontal layering that subdivides the aragonite mineral phase seems quite similar across all the pearls sampled, whatever the morphology of the concomitant radial organic structures. BSE observation appears remarkably efficient in revealing the very first traces of horizontal organic layering, which may occur far before the perfect nacreous mineralization. As purely organic components generate much weaker responses compared to mineralized areas, even the thinnest horizontal organic layers are made visible (Figs. 6b to 6i). Additionally, it should be noted that in practically all cases these initial organic layers are neither continuous nor strictly parallel. More or less elongated radial expansions still exist, which are sometimes quite short (Figs. 6b, c), but sometimes reach up to 25–30 µm height (Figs. 6d and 6g). In such cases, these radial expansions resemble prism envelopes, but the thin horizontal layering already exists between them. Clearly at that early developmental phase of aragonite mineralization, just above the initial organic layer (i.e., about one month after grafting), these two distinct organic components (radial and horizontal) can be simultaneously produced by the pearl-sac epithelium.

This initial horizontal layering is made of gently undulating laminae (Figs. 6c, 6f and 6h). The progressive shift from early layering occurs between the radial organic expansions to the true nacreous layering (Figs. 6h, i). Figure 6h, an image of the top of the radial organic digits, shows that the initial (and still undulating) horizontal layering also comprises dark spots of organic materials (arrows). The lower part of Figure 6i shows a similar pattern (level marked by arrow 1). Later, the organic spots disappear (arrow 2) and, at level 3, regularly parallel nacreous layering is obtained.

3.5 Production of prismatic calcite structures creates an additional factor of structural diversity in the concomitant aragonite areas

Figure 7 illustrates this very frequent case: calcite prisms have grown in perfect continuity (Fig. 7a, left), as shown by the regularity of their organic envelopes. In contrast, the aragonite area shows surprising variations in morphology of the organic

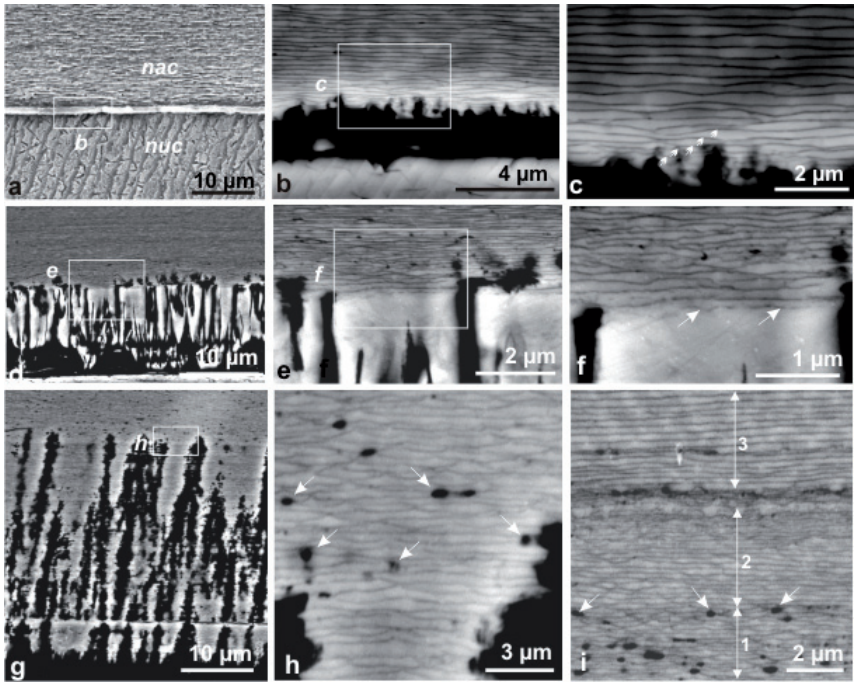

Fig. 6. Examples of various types of layering in the aragonite deposits of three different pearls. All pictures (except 6a) are from BSE imaging. 6a–c: the close to theoretical development of a nacreous pearl bed, viewed by SEM (6a): nucleus (*nuc*) covered by an organic layer, followed by nacre (*nac*). Development of horizontal organic layering made visible by BSE (6b and c): the first organic layers (arrows) are irregularly undulating, but rapidly become better coordinated and parallel (upper part of the field view). 6d–f: a rather similar sequence with much higher radial structures built by coalescence of the organic secretions. 6g–i: example of layering concomitant with expanded radial structures. Between the organic columns (6g) the horizontal layering is produced (6h) with simultaneous isolated spots of compact organic material (arrows). The progressive changes in the horizontal organic layering are shown in Figure 1i, from its lower part (1) characterized by persistence of compact organic spots, followed by a zone with an irregular pattern (2) and typical nacreous layering (3).

envelopes. They successively exhibit prismatic organization (Fig. 7a: arrow 1), followed by a typical "chevron" mode (Fig. 7a: arrow 2 and 7e, lower part), and finally a radial digit-like type (Fig. 7a: arrow 3 and 7e, upper part). It is important to note that the formation of the nacreous layer occurs by progressive change of this third pattern of organic distribution (Fig. 7f), following a process that closely resembles what is shown in Figure 6. Concomitant radial and horizontal distributions of the organic materials in the aragonite "pre-nacre" level are displayed (Figs. 7g, h).

The possible concomitance in formation of prismatic calcite prisms and true nacreous tablets can occur (Fig. 7a). After a period of lateral expansion, the calcite forming area regresses: thus, the different microstructural patterns, formed in the aragonite area, seem to progressively cover the calcite structure (Fig. 7d: arrows). Sometimes, regression of the calcite-producing area is so slow that, after usual duration of cultivation period (Fig. 8), calcite prisms are still visible at the pearl surface (Figs. 8f, g). In such cases, the contact line can be easily identified owing to the visible contrast between the nacreous layer and the growing surfaces of the calcite prisms (Fig. 8f). On axial sections, the contact surface between calcite and nacre allows a precise reconstruction of pearl history (Fig. 8g). In these slowly evolving types of pearl development, calcite prisms with lengths in the millimetre range can be observed (Figs. 8i, j).

4 Discussion: comparison of major structural patterns in pearls and shells

The adequacy of the theory that views pearls as "reversed shells" can now be tested by comparing structural and/or chemical data obtained on the different developmental stages of pearls with the corresponding sequence of events during shell formation in *Pinctada margaritifera* v. *cumingi*.

4.1 Absence of mineralogical and microstructural control in the initial mineralization stages of pearl formation

Observed at its outer margin, a juvenile shell of *Pinctada margaritifera* (Figs. 9a, b) shows the first formed calcite prisms at their very early stages (Figs. 9c–e). Between crossed

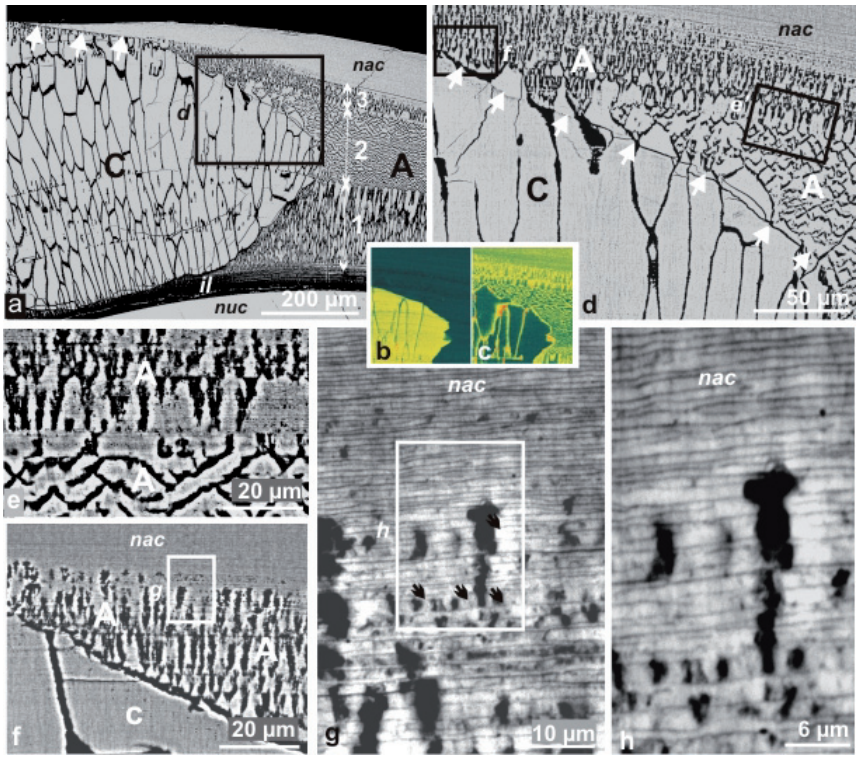

Fig. 7. Size and shape variations of the structural units in aragonite areas before shift to nacre formation. All pictures (except 7b, c) are from BSE imaging. 7a: a typical example of the developmental sequence comprising an initial organic layer (*il*, black onto nucleus surface) covered by a mixed structure: calcite prisms are on the left side and aragonite on the right. 7b, c: distributions of sulphated polysaccharides (7b) and protein sulphur (7c) provide an addition example of the correlation between calcite/aragonite mineralization and associated organic compounds (synchrotron based X-ray absorption maps). Note the clear cut opposite patterns in calcite, which is strictly linked to polysaccharides, and aragonite, where proteins are predominant, and the envelopes built on both sides. 7d–f: an enlarged view of the sequence shown in Figure 7a emphasizes the variability of organic structures resulting from coalescence of organic compounds forming envelopes. Passage from chevron to radial mode is shown in Figure 6e whereas progressive regression of this last radial mode being replaced by a pre-nacre layered mode is shown in Figure 7f. 7h, i: formation of horizontal layering is concomitant with the distal part of the radial organic structures, finishing by isolated spots (compare with Figs. 6g–i).

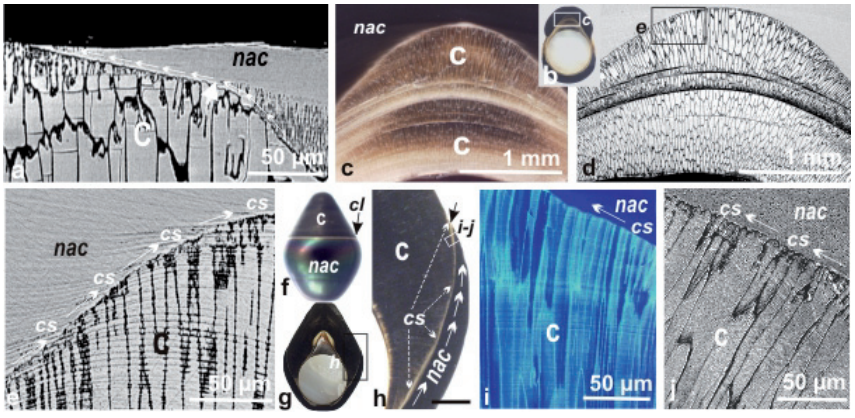

Fig. 8. Occurrence of very long calcite prisms coexisting with nacre formation; evolution of the contact surface between prisms and nacre over time. 8a: enlarged sector from Figure 7a, showing the migration of the contact line separating production of calcite prisms and nacre (arrows). 8b–e: alteration of pearl sphericity is mostly due to long term concomitant development of calcite prisms (8b, d) and nacre. Enlarged view of the frontier between prism and nacre areas (8e) shows the regular displacement of the contact surface between the two mineralizing zones. 8f–j: a rather rare example of pearl with calcite prism area (*c*) and nacreous area (*nac*) visible on the specimen surface. On a transverse section (8g), position of the contact line (8f: *cl*) appears to result from a slow but regular migration of the contact line through pearl development, forming the contact surface (8h: *cs*) between prisms and nacre (8i, j).

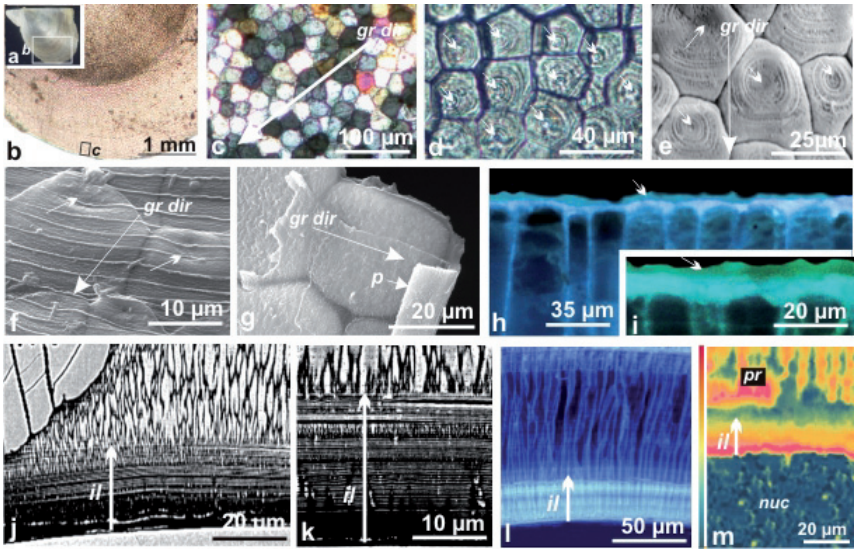

Fig. 9. Microstructure of a juvenile *Pinctada* shell compared with basal layers of pearl. 9a–c: growing edge of a shell about one month in age (9a, b). Prisms appear as polygonal units, each with monocrystalline behaviour (9c). Change in polarisation colour shows that thickness increases through time (*gr dir*: direction of growth). 9d–g: upper surfaces of the prisms are marked by a series of concentric growth rings, clearly visible in transmitted light (d) and by SEM (9e). Note the position of the centres of crystallization (arrows). 9f, g: external (f) and internal surfaces (9g) of the young prisms. On these well preserved shells, fragile organic compounds are still visible: fine organic ridges show the stepping growth mode of the periostracum and the curvature of the periostracum itself at the growing edge of the shell. (*p*: periostracum; *gr dir*: growth direction). 9h, i: the double structure of the periostracum as shown by UV fluorescence: the outer part is the protective layer, while the internal one is involved in mineralization of the very upper part of the prisms. 9j–m: structure and compositional change of the basal pearl layer: BSE pictures (9j, k) of the layered structure of a basal pearl layer. In addition to variable structure, composition also changes through time, as shown by variation in UV fluorescence and synchrotron-based XANES mapping of protein distributions (9l–m). In the four last pictures, arrows indicate the initial secretion layer (*il*), whose lower surface is in contact with nucleus surface (*nuc*) and whose upper limit is marked by occurrence of pearl-bed microstructures (*pr*: prisms).

nicols, these polygonal units, of 25–30 µm in diameter, exhibit mono-crystalline behaviour. They are about 3 µm thick (grey colour on the polarization scale) at the growing edge and their thickness increases from the margin to inner areas of the shell (Fig. 9c: arrow). Surprisingly, despite this monocrystalline behaviour, each prism shows a concentric growth pattern on its external surface (Figs. 9d–e). Obviously, the first produced mineral phase spreads from the centre of each prism. On these pictures, we also see the small circular dips in which centres of crystallization are located on the external shell surface (Figs. 9e–f: arrows) after having been transported onto the internal surface of the periostracum, which acts as a conveyor-belt. In the formation of the *Pinctada* prisms, this role is illustrated by Figure 9f, which shows a series of parallel ridges corresponding to the stepping growth mode of the periostracum. As pointed out by Saleuddin (1974), based on an electron microscopy study of periostracum structure, one of the essential roles of this organic layer is to provide the growing edge of the shell with biochemical compounds needed for early calcification. UV fluorescence of a section of shell margin, perpendicular to the external surface, allows a distinct view of the two main layers of the periostracum (Figs. 9h, i). The external layer (formed by the specialized cells of the mantle groove) is weakly fluorescent, in contrast to the internal layer, which is highly reactive to UV light. The external layer has a protective function whereas the internal one, formed during transit of the external periostracum against the outer mantle folder, contains the mineralizing compounds (for a generalized description and figure of this process, see Cuif et al. 2011).

Compared with this rigorous sequence of initial events occurring at the growing edge of the *Pinctada* outer layer, the basal pearl bed appears quite different even when, in agreement with Kawakami's observations, pearl formation starts with formation of calcite prisms. Instead of a periostracum made of a single thin protein monolayer internally covered by the first mineralizing matrices that invariably produce calcite prisms, BSE imaging reveals that the initial layer deposited onto the nucleus surface is built of a series of thin organic layers (Figs. 9j, k). During this repeated production of organic layers, the overall composition of the epithelial secretion varies, as shown here by changes in UV fluorescence (Fig. 9l), as well as by progressive decrease in protein content, as shown by synchrotron-based mapping of protein sulphur (Fig. 9m).

A greater contrast appears when considering the mineral phases. The very first mineralization in pearls occurs during the nucleus covering sequence itself; moreover, this occurs without any microstructural control. As shown by polarizing microscope observations (Fig. 1) and X-ray micro-diffractions

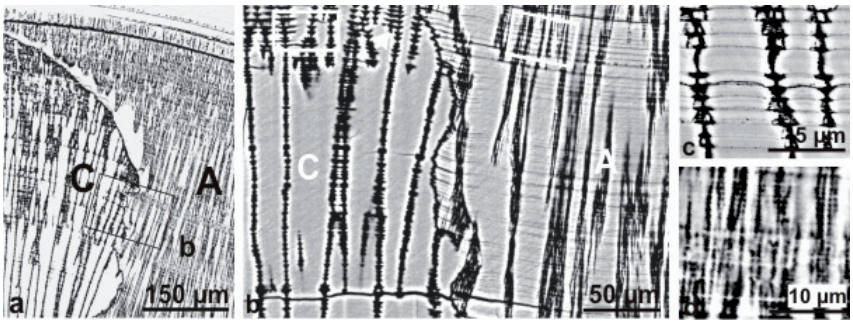

Fig. 10. Prism envelopes in the co-existing calcite and aragonite prisms (BSE imaging). 10a: a typical figure of two prismatic areas of calcite (C) and aragonite (A) growing simultaneously. 10b: at medium enlargement, morphological differences between envelopes of calcite and aragonite prisms are perceptible. 10c, d: despite the common stepping growth mode, prism envelopes exhibit distinct morphological patterns. Calcite compartments (10c) are much better defined than the aragonite ones (10d).

(Fig. 2), the basal layer of pearls may comprise both calcite and aragonite dispersed as irregular spots, showing that early secretion of the basal epithelium of the pearl-sac is all but regular. Such a simultaneous occurrence of dispersed crystals belonging to the two Ca-carbonate polymorphs shows that the organic substances produced by initial epithelial secretions include compounds enabling them to produce the mineral, but are still lacking the complementary organic assemblages required for the formation of the microstructural unit envelopes. When these envelopes are produced, far from leading to a normal shell sequence with prisms and nacre, formation of prismatic envelopes reinforces the contrast between pearls and shells. As calcite and aragonite coexist as dispersed particles in the basal layer, they may also occur in the form of radial prisms.

4.2 Prisms in shells and pearls: differences in mineral phases and organic envelopes

Numerous studies have investigated the structural properties of the prisms of *Pinctada* shells (Taylor et al. 1969; Dauphin et al. 2003; Kobayashi 2008; Okumura et al. 2010), mostly focusing on the organic components associated with the mineral phase, while organic envelopes have been less studied (Dauphin et al. 2010). In recent years, much attention has been drawn to biochemical compositions of associated organic compounds (Suzuki and Uozumi 1981; Dauphin 2003; Dauphin et al. 2003a, 2003b, 2008; Zhang et al. 2006; Suzuki et al. 2007; Kong et al. 2009; Tagaki and Miyashita 2010). Prisms of *Pinctada* shells are always made of calcite, from their very early crystallization stage (Baronnet et al. 2008) up to their final stages. At the final stage of shell development, the growth surfaces (internal side of the shell) are covered by the development of an insoluble film, with specific biochemical properties that have been recently demonstrated (Farre et al. 2011).

No records of aragonite prisms have been made so far for the shells of *Pinctada* or other bivalves belonging to the order Pteriomorpha. It is important to emphasize the contrast between calcite and aragonite prisms in pearls with respect to biocrystallization. Calcite prisms form coherent crystallographic structures through tens or hundreds of biomineralization cycles (see backscattered electron diffraction data by Perez-Huerta, in Cuif et al. 2008). Conversely, aragonite mineral units do not form radial crystals as calcite does. Although they are gathered in radial envelopes, they remain uncontrolled with respect to crystallographic orientation. This clearly suggests that the factor ensuring crystallographic consistency or mineral particles in calcite prisms is lacking for aragonite. A clear correlation exists between formation of calcite prisms and sulphated polysaccharides (Fig. 5). Calcite prisms in pearls are therefore quite similar to shell prisms with respect to mineralogy, crystallography and morphology. Aragonite prisms, in contrast, are not normally produced in *Pinctada,* so no biochemically equivalent resource exists in the mantle cells of the prismatic zone to enable the production of an organic phase capable of controlling the crystallographic orientation of aragonite particles.

The absence of this specific organic phase results in endless diversity in morphology of insoluble envelopes in the aragonite compartments (e.g., Figs. 7a and 7d–f). When prism envelopes seem the most perfectly prismatic in aragonite areas, closer BSE pictures (Fig. 10) reveal that envelopes of the aragonite radial units are multi-laminated, with imprecise limits and lack continuity through time (Fig. 10b: right side). Enlarged views (Figs. 10d, e) show the common stepping growth mode of these envelopes, but also the obvious differences in morphology of the resulting compartments (growth layers).

Some parallels can be drawn between this imperfect morphological pattern of insoluble envelopes and the randomly oriented microcrystalline aragonite units. A badly crystallized mineral phase corresponds to a weakly controlled process of envelope formation. In conclusion, with respect to the "reversed shell" theory, presence of these aberrant aragonite prism-like units appears to be a major obstacle.

4.3 Nacre settlement in *Pinctada* shells and pearls

With respect to nacre occurrence, pearls offer a remarkably wide range of variation but, in most cases, regulation finally occurs in the mineralizing mechanism of the pearl sac

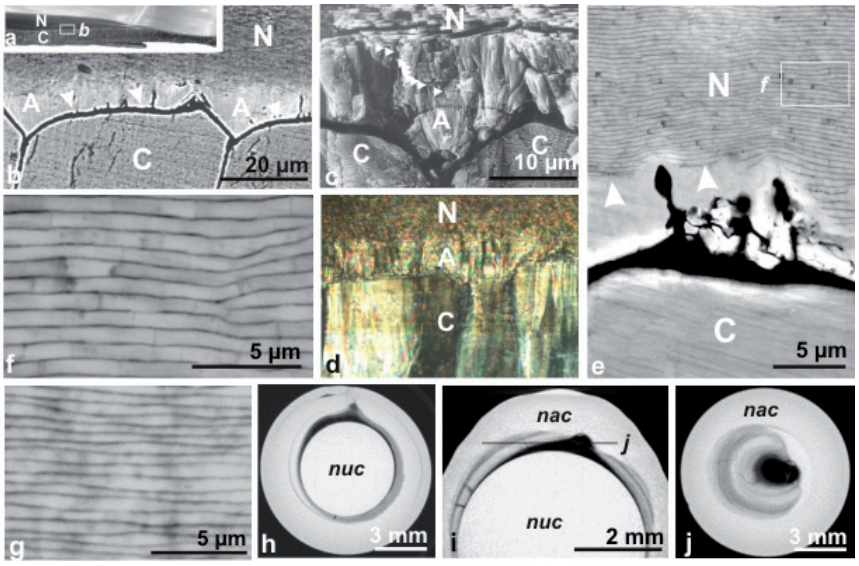

Fig. 11. Main views of nacre settlement in *Pinctada* shell compared to pearl nacre and overall structure. 11a–b: main patterns of prism/nacre transition in *Pinctada*. 11a: part of a shell section showing the two main layers (calcite prisms outside and nacreous layer within). 11b: BSE picture of the transitional steps between prisms and true nacre: calcite prisms (C) and nacre (N) are separated by a thick organic film (11b: arrows) and non-layered aragonite (A). 11c, d: before the formation of true nacre (N), the irregular aragonite layer (A) is made of well crystallized fibres (c: SEM, d: polarizing microscope). Progressive occurrence of nacreous layering is visible within the aragonite fibres (11c: arrows). 11e: from the thick organic film covering the growth surface of the prism, elongated protuberances are formed in the undifferentiated aragonite. 11f, g: BSE imaging of nacre tablets in shells (11f) and the much thinner nacre of pearls (11g). 11h–j: computer-assisted tomography provides overall views of the distribution of calcareous microstructures in pearls. Precision in geometrical distribution of the different microstructures can easily be assessed at all developmental stages or the pearl, allowing precise reconstruction of growth patterns without destroying the samples.

epithelium, resulting in the formation of nacreous mineral units. Aragonite is then organized into mineral tablets sandwiched between a series of organic laminae, mainly parallel to the nucleus surface. Variability in crystallographic orientation of nacreous tablets was recently investigated in a wide range of bivalve species including *Pinctada* (Fryda et al. 2010). A regular orientation of the c axis perpendicular to the nacreous tablets was confirmed, with some variability in directions of the a and b axes with respect to growth direction. Our observations and crystallographic characterization of aragonite behaviour in pearl beds clearly shows that the organizing factor enabling crystallographic control of aragonite particles is linked to the formation of the horizontal layering (i.e., parallel to the nucleus surface). As long as parallel horizontal membranes are not produced (this can be a matter of weeks or months for many pearls), aragonite particles remain randomly oriented. This is important evidence with respect to the hypothesis of aragonite ensuring crystallographic consistency of nacreous tablets through "holes" in the organic layers (Schäffer et al. 1997). Clearly aragonite alone is not able to self-organize into crystal-like structures.

More generally, this study of pearl layer development clearly demonstrates that production of calcite and aragonite as mineral phases and occurrence of calcite prisms or nacreous tablets as well controlled microstructural units are distinct processes that can be separated by a very long period of time (i.e., several months) during pearl formation.

Interestingly, when looking at the transitional sequence between calcite prisms and well formed aragonite in the shell of *Pinctada margaritifera* (Figs. 11a to 11d), the path is all but direct (Dauphin et al. 2008). After the enclosure of the prism growth surface by a thick organic film, a layer of non-nacreous aragonite is formed (Fig. 11b). In contrast to the early aragonite phase of the pearls, which is always made of randomly oriented microgranules, early aragonite in shells is deposited as fibrous fan systems (Figs. 11c, d). Thus, compared to the calcite/aragonite transition in pearls, the thick organic layer covering the calcite prisms and the well crystallized aragonite fibres of the *Pinctada* shell also establish a marked difference between shell and pearls. It is worth noting the irregular organic finger-like expansions growing from the prism covering layer (Fig. 11e) and the progressive deposition of the first nacreous organic film within the aragonite fibres (Fig. 11c: arrows): both structures are clear illustrations of the complexity and duration of the calcite/aragonite transitional process in shells.

With respect to shell/pearl comparison, nacreous settlement in *Pinctada* shells is always under the overall control of the animal: variations visible in the transitional step are limited in both time and space. The opposite is true for pearls: the highly variable duration of the nacreous settlement (sometime not occurring at all) clearly demonstrates the absence of an effective regulation mechanism.

Thus, far from being a simple "reversed shell", the pearl bed appears to be a complex structure of which the main

structural characteristic is *variability*. In contrast to shell organization, in which production of calcite and aragonite appears in very regular sequence, diversity occurs immediately in pearls, in both space and time. This indicates that, although entirely covered by mineralizing tissue resulting from graft development, this tissue is far from homogenous with respect to its mineralizing potential. Structural and chemical results converge to emphasize the surprising differences in cellular secretion areas, with presently unexplained differences between neighbouring sectors covering the nucleus. In some ways the "regeneration" process hypothesized by Kawakami is a more appropriate concept to summarize what occurs during pearl formation, but it does not result in formation of regular reverse sequence of events.

Regeneration of the pearl sac epithelium is a long and presently unpredictable process, leading the pearl-sac to produce very diverse and sometimes aberrant materials. With respect to pearl production, this conclusion emphasizes the need to establish a better relationship between the detailed analysis of grafting operations and characteristics of the pre-nacreous development of pearl beds. Recent improvements in X-ray computer assisted tomography allow this technique to provide an ideal platform for such an investigation, applying a statistical but non destructive approach. Figures 11h–j shows that early deposited structures exhibit significant differences in X-ray absorption coefficients, allowing an overall approach to the duration of the non-nacreous episode, and a three-dimensional reconstruction of the different layers deposited during this period. By coupling such fine scale structural studies with a better knowledge of the nanoscale structural and X-ray absorption properties of various pearl materials, a better large-scale non-destructive investigation on pearl-sac behaviour could be carried out, leading to an improved proportion of valuable pearl products.

5 Conclusion

In agreement with Kawakami's views, the mineralizing cells of the graft undergo deep metabolic changes during the post-grafting proliferation stage, which results in complete wrapping of the nucleus surface.

Considering formation of nacre in the pearl layer as an indicator of the end of the recovery period, we can observe a great diversity in the duration of this period: from immediate recovery to several months of non-nacreous mineralization.

With respect to mineralogy, microstructure and the biochemical composition of the associated organic compounds, materials produced before the return to nacreous formation show a great diversity, even within a single pearl bed, sometimes leading to formation of abnormal combinations such as prismatic microcrystalline aragonite. The results of our microstructural investigations do not show a regular sequence of mineralization events, indicating that we should not consider pearls as "reversed shells". An improved understanding of the factors influencing this erratic recovery process, which has highly negative effects on pearl layer development, should significantly improve the proportion of valuable products obtained from pearl farming.

Acknowledgements. Authors thank the managing team of the ADEQUA program for allowing publication of the present data. ADEQUA is a long-term research project funded by the Polynesian administration for Fisheries and Aquaculture, involving 11 technical and scientific teams studying intracellular and extracellular aspects of the mineralization processes responsible for pearl formation and quality. Funding support was also provided by ESRF (EC208, EC545 grants). The authors are also grateful to referees (A. Perez-Huerta and anonymous) for their valuable contributions.

References

Arnaud-Haond S., Goyard E., Vonau V., Herbaut C., Prou J., Saulnier D., 2007, Pearl formation: persistence of the graft during the entire process of biomineralization. Mar. Biotechnol. 9, 113–116.

Baronnet A., Cuif J.P., Dauphin Y., Farre B., Nouet J., 2008, Crystallization of biogenic Ca-carbonate within organo-mineral microdomains. Structure of the calcite prisms of the pelecypod *Pinctada margaritifera* (Mollusca) at the submicron to nanometer ranges. Mineral. Mag. 72, 617–626.

Cuif J.P., Ball A.D., Dauphin Y., Farre B., Nouet J., Perez-Huerta A., Salomé M., Williams C.T., 2008, Structural, mineralogical and biochemical diversity in the lower part of the pearl layer of cultivated seawater pearls from Polynesia. Microsc. Microanal. 14, 405–417.

Cuif J.P., Dauphin Y., Sorauf J.E., 2011, Biominerals and fossils through time. Cambridge University Press.

Cuif J.P., Dauphin Y., Doucet J., Salomé M., Susini J., 2003, XANES mapping of organic sulfate in three scleractinian coral skeletons. Geoch. Cosmoch. Acta, 67, 75–83.

Dauphin Y., 2003, Soluble organic matrices of the calcitic prismatic shell layers of two pteriomorphid Bivalves: *Pinna nobilis* and *Pinctada margaritifera*. J. Biol. Chem. 278, 15168–15177.

Dauphin Y., Cuif J.P., Doucet J., Salomé M., Susini J., Williams C.T., 2003a, In situ chemical speciation of sulfur in calcitic biominerals and the simple prism concept. J. Struct. Biol. 142, 272–280.

Dauphin Y., Cuif J.P., Doucet J., Salomé M., Susini J., Williams C.T., 2003b, In situ mapping of growth lines in the calcitic prismatic layers of mollusc shells using X-ray absorption near-edge structure (XANES) spectroscopy at the sulphur edge. Mar. Biol. 142, 299–304.

Dauphin Y., Ball A.D., Cotte M., Cuif J.P., Meibom A., Salomé M., Susini J., Williams C.T., 2008, Structure and composition of the nacre – prism transition in the shell of *Pinctada margaritifera* (Mollusca, Bivalvia). Anal. Bioanal. Chem. 390, 1659–1169.

Dauphin Y., Brunelle A., Cotte M., Cuif J.P., Farre B., Laprévote O., Meibom A., Salomé M., Williams C.T., 2010, A layered structure in the organic envelopes of the prismatic layer of the shell of the pearl oyster *Pinctada margaritifera* (Mollusca, Bivalvia). Microsc. Microanal. 16, 91–98

Farre B., Brunelle A., Laprévote O., Cuif J.P., Williams C.T., Dauphin Y., 2011, Shell layers of the black-lip pearl oyster *Pinctada margaritifera*: matching microstructure and composition. Comp. Biochem. Physiol. B 159, 131–139.

Fryda J., Kliknarova K., Frydiva B., Mergl M., 2010, Variability in the crystallographic texture of bivalve nacre. Bull. Geosci. 85, 645–662.

Inoue N., Ishibashi R., Ishikawa T., Atsumi T., Aoki H., Komaru A., 2011, Can the quality of pearls from the Japanese pearl oyster (*Pinctada fucata*) be explained by the gene expression patterns of the major shell matrix proteins in the pearl sac? Mar. Biotechnol. 13, 48–55.

Joubert C., Piquemal D., Maris B., Manchon L., Pierrat F., Zanella-Clleaon I., Cochennec-Laureau N., Guegen Y., Montgnani C., 2010, Transcriptome and proteome analysis of *Pinctada margaritifera* calcifying mantle and shell: focus on biomineralization. BMC Genomics 11, 613 doi:10.11861471-2164-11-613.

Kawakami I.K., 1952a, Studies on pearl formation. On the regeneration and transformation of the mantle piece in the pearl oyster. Mem. Fac. Kyushu Univ., Ser. E 1, 83–89.

Kawakami I.K., 1952b, Marine regeneration in pearl oyster (*Pinctada martensii*). J. Fuji Pearl. Inst. 2(2), 1–4.

Kobayashi I., 2008, Scanning electron microscopic structure of the prismatic layer in the Bivalvia. Front. Mater. Sci. China 2, 246–252.

Kong Y., Jing G., Yan Z., Li C., Gong N., Zhu F., Li D., Zhang Y., Zheng G., Wang H., Xie L., Zhang R., 2009, Cloning and characterization of prisilkin-39, a novel matrix protein serving a dual role in the prismatic layer formation from the oyster *Pinctada fucata*. J. Biol. Chem. 284, 10842–10854.

Nudelman F., Shimoni E., Klein E. , Rousseau M., Bourrat X., Lopez E., Addadi L., Weiner S., 2008, Forming nacreous layer of the shells of the bivalves *Atrina rigida* and *Pinctada margaritifera*: an environmental- and cryoscanning electron microscopy study. J. Struct. Biol. 162, 290–300.

Okumura T., Suzuki M., Nagasawa H., Kogure T., 2010, Characteristics of biogenic calcite in the prismatic layer of a pearl oyster, *Pinctada fucata*. Micron 41, 821–826.

Rouzière S., Jourdanneau E., Kasmi B., Petermann D., Albouy P.A., 2010, A laboratory X-ray microbeam for combined X-ray diffraction and fluorescence measurements. J. Appl. Cryst. 43, 1131–1133.

Saleuddin A.S.M., 1974, An electron microscopic study of the formation and structure of the periostracum in *Astarte* (Bivalvia). Rev. Can. Zool. 52, 1463–1471.

Schâffer T.E., Ionescu-Zanetti C., Proksch R., Fritz M., Walters D.A., Almquist N., Zaremba C., Belcher A.M, Smith B.L., Stucky G.D., Morse D.E., Hansma P.K., 1997, Does abalone nacre form by heteroepitaxial nucleation or by growth through mineral bridges. Chem. Mater. 9, 1731–1740.

Suzuki S., Uozumi S., 1981, Organic components of prismatic layers in molluscan shells. J. Fac. Sci. Hokkaido Univ., Ser. IV. 20, 7–20.

Suzuki M., Sakuda S., Nagasawa H., 2007, Identification of chitin in the prismatic layer of the shell and a chitin synthase gene from the Japanese pearl oyster, *Pinctada fucata*. Biosci. Biotechnol. Biochem. 71, 1735–1744.

Suzuki M., Saruwatari K., Kogure T., Yamamoto Y., Nishimura T., Kato T., Nagasawa H., 2009, An acidic matrix protein, Pif, is a key macromolecule for nacre formation. Science 325, 5946, 1388–1390.

Tagaki R., Miyashita T., 2010, Prismin: A new matrix protein family in the Japanese pearl oyster (*Pinctada fucata*) involved in prismatic layer formation. Zool. Sci. 27, 416–426.

Taylor J.D., Kennedy W.J., Hall A., 1969, The shell structure and mineralogy of the Bivalvia. I. Introduction. Nuculacae–Trigonacae. Bull. Br. Mus. Nat. Hist. Zool. 3, 1–125.

Taylor J., Strack E., 2008, Pearl production. In: Southgate P.C., Lucas J.S. (Eds.). The pearl oyster, Amsterdam, Elsevier, pp. 272–302.

Tsukamoto D., Sarashina I., Endo K., 2004, Structure and expression of an unusually acidic matrix protein of pearl oyster shells. Biochem. Biophys. Res. Comm. 320, 1175–1180.

Zhang C., Xie L., Huang J., Liu X., Zhang R., 2006, A novel matrix protein family participating in the prismatic layer framework formation of pearl oyster, *Pinctada fucata*. Biochem. Biophys. Res. Comm. 344, 735–740.